

11 SECONDARY MIRRORS

11.1 Overview

There will be two Gregorian secondaries for the GMT. One is an adaptive secondary mirror (ASM) with deformable thin facesheets and the other a fast-steering secondary mirror (FSM) with rigid segments. Both are 3.25 m in diameter and built as seven separate, circular segments with the same geometry as the primary segments. The seven segments will be conjugated 1:1 to the segments of the primary. Figure 11-1 shows the structural concept, which is the same for both secondaries. The support for the segments is largely hidden behind the optics, so the view from the instrument shows mostly sky around each segment, for optimal sky baffling in the thermal infrared. The gaps between the secondary segments also ensure that the beam from one primary segment strikes only the conjugated secondary segment for a field up to 10' radius. The seven segments are held together to form a single parent ellipsoid, through a rigid truss with adjustable hexapod connections for each segment. The truss itself is held relative to 3 points at the top of the telescope structure by a single large adjustable hexapod.

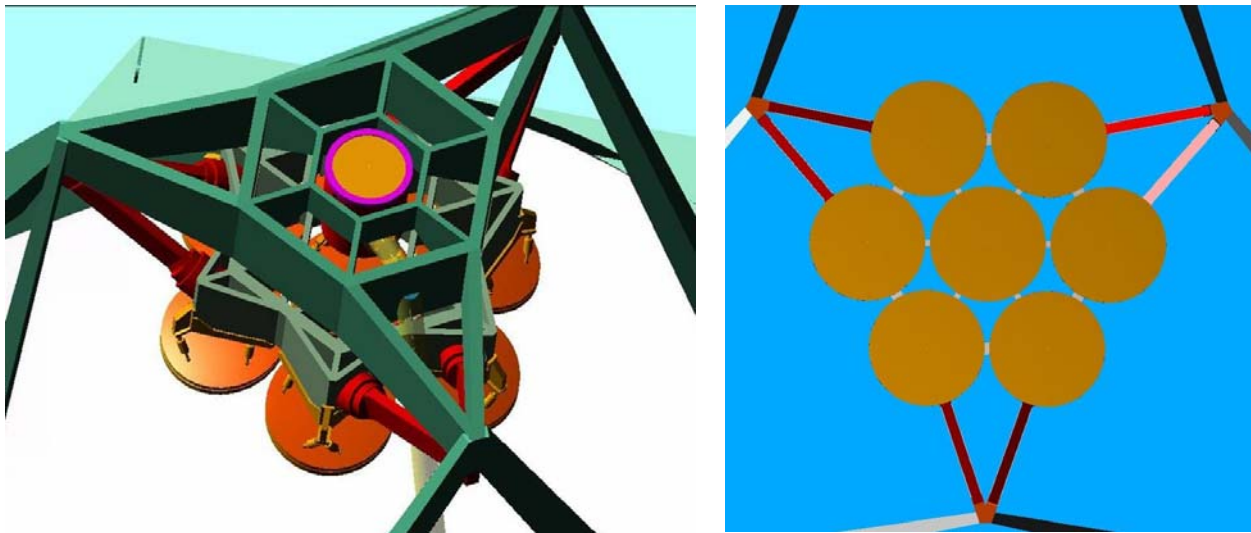


Figure 11-1. Schematic views of the GMT secondary mirror and its support system from above (left) and from the instrument (right). Viewed from the instrument, the support structure is almost entirely hidden behind the mirror.

The ASM will be used for both adaptive optics and seeing-limited operation. For seeing-limited work, the segments are commanded to take on an accurate figure without continuous feedback from a wavefront sensor. This is possible because the shape of the deformable facesheet is controlled relative to a stiff reference body; after a single shape calibration the ASM can hold the accurate shape with only slow wavefront feedback to correct for gravity deflection of the reference body. Thus the switch from adaptive to seeing-limited operation is possible without a change of secondaries.

The FSM has lightweight rigid segments and will be used for seeing-limited operation only. The FSM segment supports are capable of producing rapid, small tip-tilt motions to compensate for wind-induced excitation of the lower resonant frequencies of the telescope at about 8 Hz. These motions will be necessary under unfavorable wind conditions.

The FSM will be the first secondary implemented on the GMT. It will be used in the initial engineering phase and commissioning of the telescope so that we can first address the alignment of the seven primary and seven secondary segments before dealing with the additional degrees of freedom introduced by the deformable segments. It will also be used for seeing-limited observations at times when the ASM needs to be removed for maintenance or repair. The FSM will be used mostly in the visible, so its coating may favor shorter wavelengths, with very high reflectivity down to 300 nm. The ASM will use the best universal coating, which may involve some loss below 400 nm.

At present, the only operating adaptive secondary mirror is at the MMT. The MMT adaptive secondary, shown in Figure 11-2, is similar to the LBT design described below. The mirror is 640 mm in diameter. The shell has an average thickness of 2.0 mm and is controlled by 336 actuators.

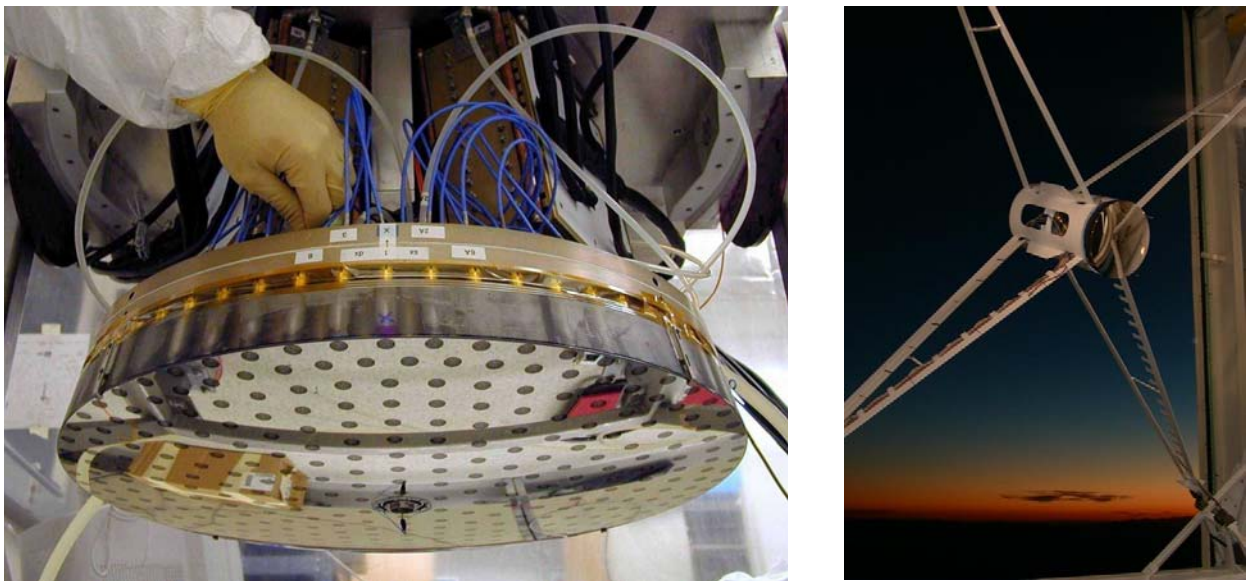


Figure 11-2. MMT adaptive secondary mirror in the lab before coating (left) and in the telescope (right).

Two more adaptive secondary mirrors are being manufactured for the twin 8.4 m LBT. Each LBT secondary consists of a thin Zerodur shell, 911 mm in diameter with an average thickness of 1.6 mm, whose shape is controlled by 672 actuators. The actuators are electromagnets acting against small permanent magnets attached to the rear surface of the shell. The actuators support the weight of the shell, so there is no mechanical contact except for a central membrane that constrains the shell laterally. An annular capacitive sensor surrounds each actuator to measure the gap between the shell and a rigid reference body. This signal, read at about 100 kHz, provides high-speed feedback to turn the force actuator into a position actuator with a bandwidth greater than 1 kHz and precision of 3 nm. In adaptive mode, the position commands are updated based on wavefront measurements. The bandwidth of this outer loop is determined by the wavefront measurement and is approximately 50 Hz. The step response time for the mechanical system—the actuators and shell—is less than 1 ms.

The actuator system for the LBT secondaries is being set up at the Arcetri Observatory while the Zerodur shells are being manufactured at the University of Arizona. One significant difference

between the LBT and MMT adaptive secondaries is that the LBT system is capable of operating with a larger gap between the shell and the reference body (up to 100 μm , vs. 40 μm for MMT) in order to accommodate chopping by up to $\pm 5''$ with the deformable mirror. This chopping capability is made possible in part by the introduction of electronic damping to replace viscous damping by air in the narrow gap of the MMT system. Electronic damping also allows the actuator control loop to operate with a higher gain and hence higher bandwidth. Tests with a 45-actuator prototype system at Arcetri have demonstrated the response and accuracy of the system with electronic damping.

The segments of the GMT adaptive secondary are similar to the LBT secondaries. Like the LBT secondaries, the GMT segments have a chopping mode (provided by motion of the shells relative to their reference bodies) in addition to the adaptive mode and the fixed mode. Differences between the GMT and LBT designs, discussed in Section 11.3.4, include a thicker shell and a modified lateral restraint.

11.2 Secondary mirror mount

The ASM and the FSM will be mounted to the telescope in the same way, shown in Figure 11-3. The six struts of the telescope's upper support structure hold the triangular main frame of the secondary mirror mount. A sub-frame is attached to the main frame through six stiff positioning actuators, similar to the hard points that position each primary mirror segment. Each secondary mirror segment is attached to the sub-frame through a set of six fast fine-positioning actuators. The main actuators provide the coarse movement of the full secondary mirror, to correct for gravity deflections and slowly varying thermal deflections of the telescope structure. The fine actuators provide the fine movement of the secondary segments to correct for relative displacements of the secondary and primary segments. For the FSM, the fine actuators will also provide rapid tip-tilt motion of each segment, to correct for motion of the secondary mirror due to wind-induced vibration and tracking jitter. The ASM will correct for these rapid motions with the deformable mirror, while the fine actuators provide slow compensation to reduce the stroke of the deformable mirror's actuators.

Table 11-1 and Table 11-2 list range and resolution requirements for the main actuators and fine actuators, respectively. The ranges listed are adequate to compensate for alignment errors that will arise due to gravity, temperature gradients, and wind. The resolutions listed for the fine actuators in Table 11-2 are 4-5 times finer than the alignment goals for secondary segments listed in Chapter 8. At this stage of the design we do not know whether the main actuators will be able to move the sub-frame smoothly enough to meet the alignment specification, even for seeing-limited observations. The initial strategy is therefore to make large corrections with the main actuators infrequently, and make small corrections at a faster rate with the fine actuators. The ASM will make even faster corrections with the deformable mirror. The resolution of the main actuators is not critical; the values listed in Table 11-1 correspond to an achievable resolution of about 3 μm per actuator.

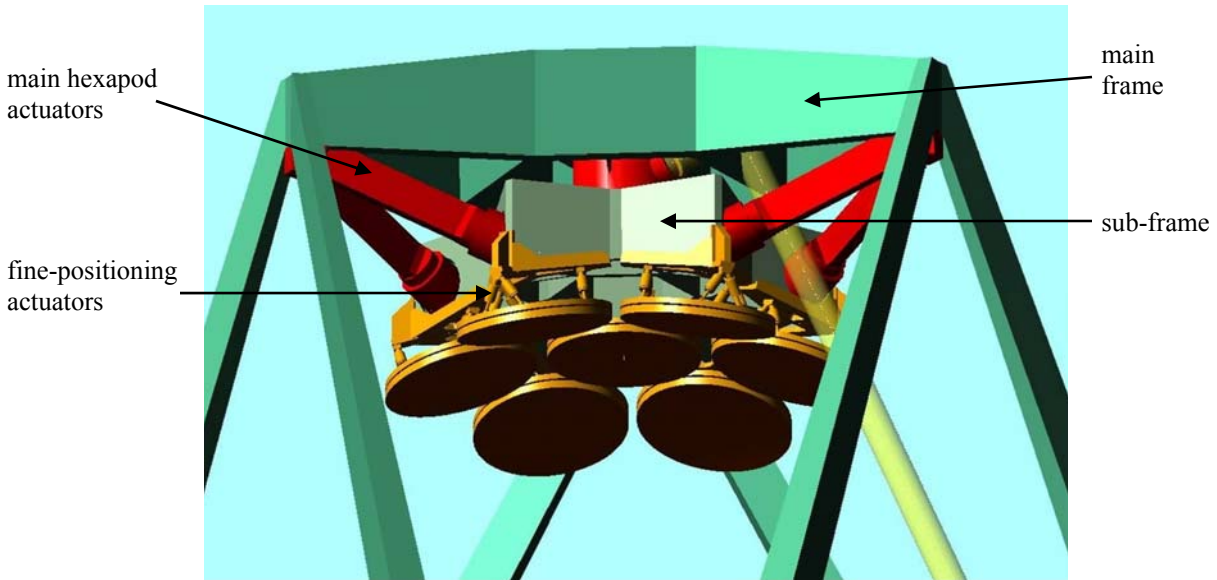


Figure 11-3. Secondary mirror mount, shown with the ASM. Essentially the same mount is used for the FSM. This view also shows the path of the sodium laser beam from the laser to the beam projector located behind the secondary mirror mount.

Table 11-1. Requirements for the main actuators. Ratio of mirror tilt to image motion is approximately 4:1.

motion	range	resolution
lateral	± 11 mm	5 μ m
axial	± 10 mm	5 μ m
mirror tilt	$\pm 7.2'$	1"
rotation	$\pm 15'$	1"

Table 11-2. Requirements for the fine actuators. Ratio of segment tilt to image motion is approximately 4:1.

motion	range	resolution
lateral	± 0.5 mm	0.2 μ m
axial	± 0.5 mm	0.2 μ m
segment tilt	$\pm 20''$	0.01"
rotation	$\pm 70''$	0.04"

The mass of the secondary mirror assembly contributes to the lowest resonances of the telescope structure. We have designed and analyzed candidate structures in which the main frame and the sub-frame are made of aluminum and of carbon fiber. The overall mass of the main frame, sub-frame, main and fine actuators, and ASM (the heavier of the two secondaries) is 6000 kg with aluminum frames or 4900 kg with carbon fiber frames. The baseline design uses carbon fiber frames in order to improve the structural performance and minimize thermal expansion of the sub-frame. The GMT modal analysis in Chapter 7 assumes a mass of 6400 kg and so is slightly conservative in this respect.

The stiffness of the main actuators affects both the local vibration modes in the sub-frame assembly (motion of the sub-frame and secondary mirrors at frequencies around 35 Hz) and to a lesser extent some lower-frequency modes of the optics support structure (motion of the entire secondary mirror assembly, including the main frame, at frequencies around 8 Hz). The main actuators will be made stiff enough that their contribution to the compliance of the lower-frequency modes of the OSS is small. A stiffness of 160 N/ μm for the main actuators—40% stiffer than the specified LBT primary mirror hard points—is a reasonable goal. This stiffness would result in only a 0.2 Hz reduction in the frequency of the lowest-frequency mode of the OSS: 7.8 Hz as opposed to 8.0 Hz for infinitely stiff main actuators.

The dynamic response analysis of Chapter 7 shows that wind shake would produce motion of the segments' images of 0.08" rms without active correction, for a 13 m/s wind (90th percentile) with the enclosure vents closed. Most of this is the pointing error, common to all segments, that occurs at frequencies in the range 8-10 Hz. For the 75th percentile wind speed of 9.5 m/s, at which the performance is to be evaluated, the image motion is reduced by almost a factor of 2 to 0.04" without correction. For the FSM, the fine actuators will correct this motion as well as the smaller errors due to tracking jitter. The image budget for natural seeing limits the residual error to $\theta_{80} = 0.11''$, with a goal of $\theta_{80} = 0.06''$. These image sizes are equivalent to rms image motion of 0.041" and 0.025", respectively, so little or no correction is needed. Table 11-3 lists specific goals for the rapid correction by the fine actuators. We expect that the modest reduction in image motion can be achieved with feedback from fast image motion sensors in the focal plane.

Table 11-3. Goals for correction of wind-induced vibration and tracking jitter with the fine-positioning actuators. Ratio of segment tilt to image motion is approximately 4:1.

range of image motion	0.5" rms
attenuation of image motion at 4 Hz	0.1
attenuation at 8 Hz	0.25
attenuation at 12 Hz	0.5

For the ASM in adaptive optics mode, the deformable mirror will correct for image motion due to all sources, including wind shake. More than an order-of-magnitude reduction in motion due to wind is required for diffraction-limited performance at 1 μm . This is a straightforward correction for the ASM provided the motion is sensed rapidly enough. We expect that the focal-plane sensors will be adequate, but we are also exploring the possibility of mounting accelerometers on the sub-frame or the segments.

11.3 Adaptive secondary mirror

11.3.1 Overview

The concept for an adaptive secondary comes from Salinari and colleagues at Arcetri Observatory (Ref. 1). It has been developed through a collaboration between Arcetri, Steward Observatory and several companies, and has been described in a series of papers (Refs. 2-9). Two companies, Microgate and ADS International, have developed a powerful implementation of the mechanics, electronics and software for the LBT adaptive secondaries, while Steward

Observatory provides the glass components. The electromagnetic actuators used for the MMT and LBT adaptive secondaries offer several advantages. No physical contact is necessary between the glass shell and the actuators or support structure, except through a central membrane for lateral restraint. The actuator stroke is not limited by mechanical constraints. This allows high order modes and tip-tilt both to be corrected by the same deformable mirror, which can also chop for background calibration in the thermal IR. The actuators have no intrinsic stiffness, this being the function of the active control, so if an actuator fails the shell approximately follows its natural curvature over the affected area.

The real-time shape control enabled by the independent position sensors allows the mirror to operate as a conventional secondary, with no intervention from the reconstructor computer or AO wavefront sensor. (Gravity deflections of the reference body will be corrected by the slow active optics loop.) In an experiment at the MMT, the adaptive secondary was commanded to hold position in the face of wind at 10 m/s. Shape deviations of 10 nm rms were observed by continuous monitoring of the capacitive sensors. The mirror has also operated successfully in closed loop in winds up to 15 m/s. This capability eliminates the need to change secondary mirrors between AO operation and natural seeing operation. Furthermore, should the AO system go offline for any reason, seeing-limited observations would still be possible.

The GMT adaptive secondary will be an evolution of the LBT design, as the LBT design evolved from the MMT design. Table 11-4 compares the properties of the MMT, LBT, and proposed GMT AO mirrors. The total mass includes electronics, estimated at 30 kg for LBT and GMT. Apart from electronics, the total mass of the GMT ASM is estimated from the LBT mass, scaled by the cube of the diameter.

Table 11-4. Comparison of adaptive secondary mirror designs for MMT, LBT, and a GMT segment.

property	units	MMT	LBT	GMT segment
shell diameter	mm	642	911	1063
shell thickness	mm	2.0	1.6	2.4
shell shape		convex hyperboloid	concave ellipsoid	concave off-axis ellipsoid
shell + magnet mass	kg	2.6	4.4	9
number of actuators		336	672	672
pupil scale factor		10.0	9.0	7.9
actuator spacing on primary	mm	310	281	281
total mass	kg	128	240	360

11.3.2 Performance of the MMT adaptive secondary

The MMT adaptive secondary mirror is the first realization of a deformable secondary mirror with AO correction. After initial engineering tests and modifications starting in June 2002, the MMT adaptive secondary has performed reliably at the telescope since January 2004. Scientific observations are being made over four times a year in two-week periods. Five papers have been published based on these observations (Refs. 10-14) with at least five more in preparation.

The MMT AO system is in the final process of being handed over to the MMT Observatory. Refinements during 2005 have reduced the manpower requirements for the AO system to just two operators. The typical time to go from acquiring a guide star to closing the loop and delivering corrected images to the science instruments is 3 minutes.

The MMT AO Strehl ratio is typically 38% at H band for 0.7" seeing in the wavefront-sensing visible bands. Figure 11-4 shows images obtained with the system. The performance is limited by vibrations in the upper framework of the telescope. Four accelerometers are being mounted on the back of the reference body to provide a feed-forward tip-tilt signal to the servo loop. This change is expected to push the Strehl ratio at H band above 50% later in 2006.

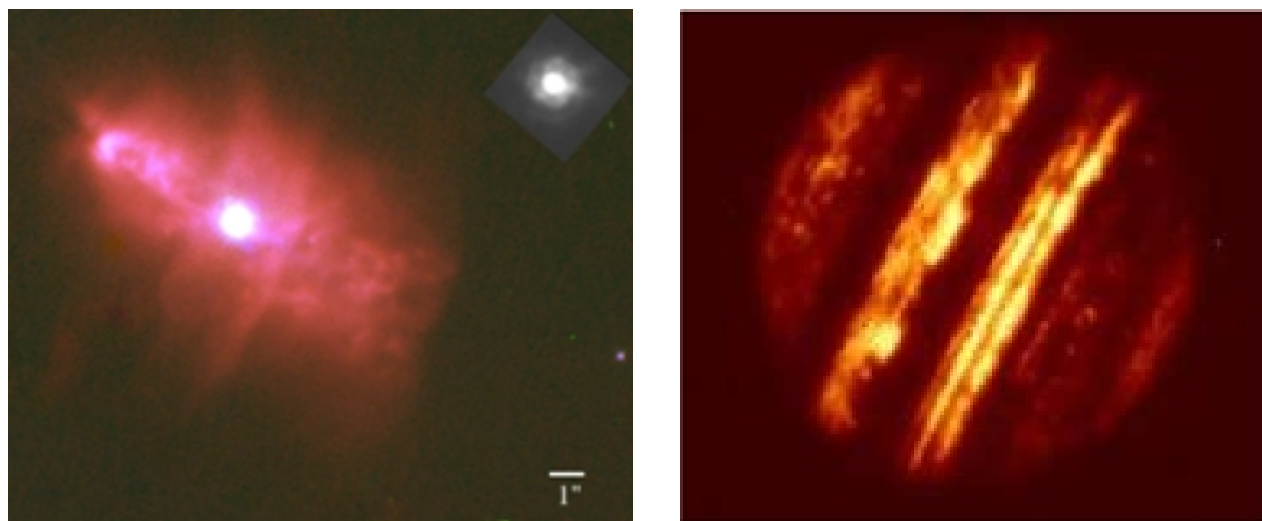


Figure 11-4. Images obtained with the MMT AO system. Left: IC 2149 at 2.2 μm , obtained with the ARIES imager. Right: Jupiter at 4.8 μm , obtained with the Clio imager.

For 2006 there are two science runs scheduled in the first trimester, and six runs per year are planned. The system has been successful in demonstrating that routine science observations can be made with a deformable secondary, delivering AO performance similar to conventional AO systems on other telescopes.

The additional advantage of delivering sensitive, high-resolution images in the thermal infrared is being exploited through the use of an 8-25 μm imager and nulling interferometer (MIRAC-BLINC; Refs. 11-12), a 3-5 μm camera (CLIO, commissioned in 2005; Ref. 13) and a 1-5 μm spectrograph (ARIES, currently being completed; Ref. 14). Laboratory tests of rapid sky chopping (5-10 Hz for a 5" throw) with continuous adaptive correction have also been carried

out with the MMT adaptive secondary. This additional mode of operation will be tested on the sky in upcoming observing runs during 2006.

11.3.3 Requirements

The fundamental requirements for the ASM, discussed in Chapter 9, are the spatial resolution, the temporal resolution or bandwidth, and the wavefront accuracy. The baseline design has 672 actuators per segment for a spatial resolution of 32 cm in the telescope pupil, the same as the LBT and enough to match the highest spatial resolution available with the NGS sensor and a 1 ms exposure. The system bandwidth—including wavefront sensing—is specified as 50 Hz for -3dB error rejection. In order to limit the residual error after correction for wind shake to 30 nm rms, a higher system bandwidth may be needed with feedback from image motion sensors. The ASM will support this system performance if its bandwidth is greater than about 500 Hz at the -3dB point. An actuator update rate of 2 kHz is also specified. The LBT ASM meets these requirements and the GMT design will have the same response or better.

The wavefront accuracy requirements for the ASM are 15 nm rms wavefront error after a full adaptive correction with all 672 actuators, and 20 nm rms wavefront after a partial correction based on wavefront measurements with subapertures of 50 cm diameter in the telescope pupil. This accuracy requirement applies almost entirely to the polished figure of the shell, because the actuators contribute an insignificant error. The polished figure may contain low-order errors with large amplitudes that will be corrected with the actuators. Correction of these permanent figure errors must use only a small fraction of the typical actuator forces used to correct seeing. Another potential source of small-scale error, gravitational print-through of the 672 actuators, will be shown to be insignificant.

For seeing-limited operation, the accuracy requirement for the secondary mirror figure is a contribution to the image size $\theta_{80} = 0.039''$, with a goal of $0.026''$. These values apply to the figure after a full 672-actuator correction based on a static wavefront calibration as described in Section 11.3.8. A segment figure meeting the adaptive optics requirement (15 nm rms wavefront) is diffraction-limited at 500 nm so it meets the goal for image size. The reference body, on a 9-point support, deflects under gravity by about 140 nm rms over the operational elevation range, or 35 nm rms after alignment aberrations are corrected by moving the segment. Most of this deflection will be corrected using a look-up table, and residual errors will be corrected with feedback from the slow active optics wavefront sensor. Static figure errors in the reference body do not contribute to the wavefront error because the position commands to the actuators are based on a static measurement of the shell's figure.

Chopping for background subtraction in the thermal IR is a valuable capability of the ASM. The goal called out in Chapter 9 is a chopping throw of $\pm 2''$ with a 90% duty cycle at 5 Hz, and continuous adaptive correction at each position. The $\pm 2''$ throw requires physical motion of the shell by $\pm 60 \mu\text{m}$ at the extreme edges of two of the secondary segments. This motion sets a lower limit to the gap between the shell and its reference body. For normal operation of the ASM, the gap would be approximately $50 \mu\text{m}$, where the capacitive sensors are most sensitive. For chopping, the mean gap would be increased to about $100 \mu\text{m}$.

The aspheric departure of the LBT secondaries is 0.13 mm peak-to-valley. The rear surface of the shell was made spherical, giving only a $\pm 4\%$ variation in thickness, not enough to affect the dynamic performance significantly. The matching surface of the reference body is therefore spherical as well. The GMT secondary segments have 1.7 mm peak-to-valley aspheric departure. Pending a more thorough analysis, we assume that both surfaces will have to be aspheric in order to maintain approximately uniform thickness. The matching surface of the reference body will therefore be aspheric as well. The accuracy requirement for these two additional aspheric surfaces is that they match within 25 μm peak-to-valley in order to provide a sufficiently uniform gap.

Additional requirements are related to reliability and maintenance. The system is inherently tolerant of actuator failures as described in Section 11.3.1, but with a total of 4600 actuators the failure rate must be controlled. The MMT secondary, after an initial loss of seven actuators, has experienced no failures in two years including more than 200 hours of operation on the sky and much more time in engineering tests. The mean time between failures (MTBF) for an actuator appears to be greater than 100,000 hours after infant mortality. In the LBT design, actuators are inserted through the reference body and into the mounting and cooling plate. Replacing an actuator therefore requires removal of the shell. If this aspect of the LBT design is carried over to the GMT ASM, actuators would not be replaced until enough have failed to have a noticeable effect on performance, on the order of 10 in a segment, and the replacement will probably involve removing the ASM from the telescope. The design goal is a MTBF of 100,000 hours, which would cause about 0.5 failure per night in the full ASM. If the actuator replacement criterion is 10 failures per segment, the ASM would be removed for actuator replacements roughly every 100 days and would be out of service for 1-2 days.

11.3.4 Design

The design of the ASM starts with the LBT design as a baseline. In fact, the LBT design meets all GMT requirements for number of actuators, bandwidth, and wavefront accuracy. A few changes are necessary or desirable due to the different diameter (1063 mm vs. 911 mm for LBT). Other changes will probably be made as the design is refined, experience is gained with the LBT system, and more powerful electronic parts become available.

Figure 11-5 shows the key components of the LBT adaptive secondary. The deformable Zerodur shell is 911 mm in diameter with an average thickness of 1.6 mm. The shell has a central hole to which a membrane is attached for lateral restraint. The position and shape of the shell are controlled relative to a stiff Zerodur reference body that is 50 mm thick. The reference body is perforated by holes for the 672 electromagnetic force actuators, which are mounted in an aluminum cooling plate behind it.

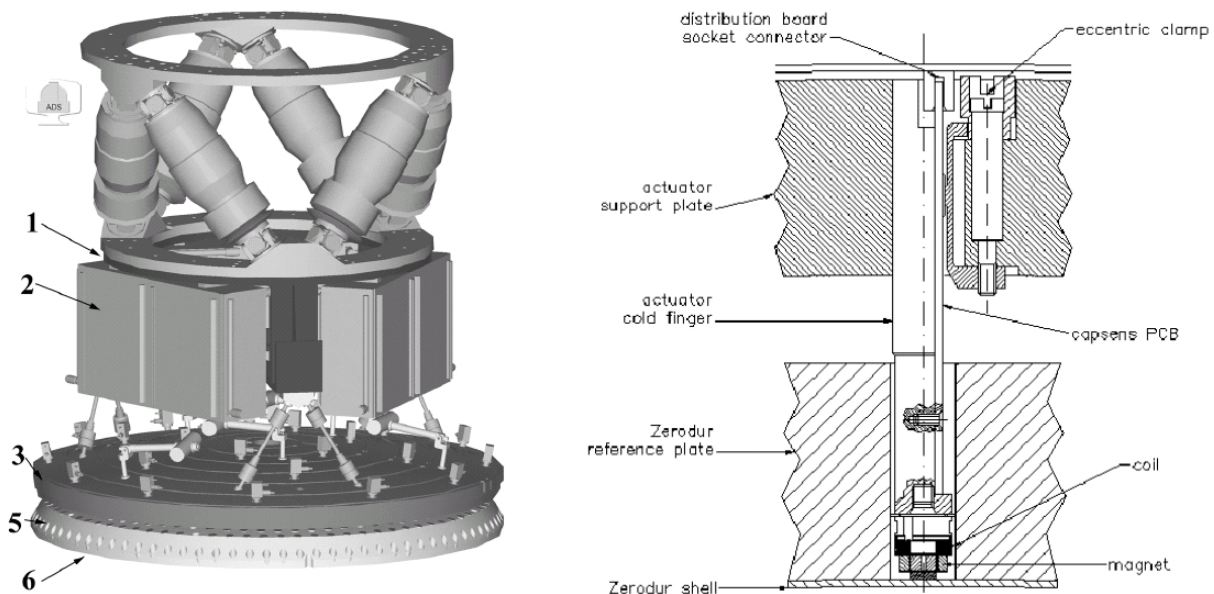


Figure 11-5. Left: LBT adaptive secondary mirror, including hexapod positioner. Components that are common to the GMT design include the actuator mounting and cooling plate (3), Zerodur reference plate (5) and Zerodur shell (6). Right: one of the 672 actuators.

Figure 11-6 shows the LBT reference body and actuator mounting plate in the lab. The actuator mounting plate contains copper tubes for a circulating coolant system that removes the heat generated by the actuators. It is supported by a fixed hexapod from a flange, (1) in Figure 11-5. This hexapod is replaced by the fine actuators in the GMT secondary segment. The reference body is supported from the actuator mounting plate through a fixed kinematic constraint with additional counterweight supports to minimize gravitational deflection. (These are not visible in Figure 11-6.)

The actuator, shown in Figure 11-7, consists of an electromagnet and a permanent magnet at the end of an aluminum post, the “cold finger”. The magnets act against a permanent magnet bonded to the rear surface of the shell. Displacement between the shell and the reference body is measured through an annular capacitive sensor surrounding the magnets. A capacitive sensor board is mounted on the cold finger. The cold finger transfers heat from the actuator and sensor board to the mounting and cooling plate.

The capacitive sensors are formed by a continuous aluminum coating on the rear surface of the shell and discrete annular coatings on the surface of the reference body, one surrounding each actuator. A 156 kHz reference signal is fed to the continuous coating, and the responses of the annular coatings are measured. The sensor board on the actuator contains a pre-amplifier and two sample-and-hold circuits whose outputs are the minimum and maximum voltage; their difference is inversely proportional to the gap. The sensor has a -3dB bandwidth of 90 kHz. It is sampled digitally at about 100 kHz with a resolution of 1.5 nm. The noise level is 2 nm rms at a gap of 50 μm . (Ref. 9)



Figure 11-6. LBT reference body and actuator mounting plate with fixed hexapod support. This photo taken in the lab has been rotated 180° to show the secondary as if the telescope were zenith pointing.

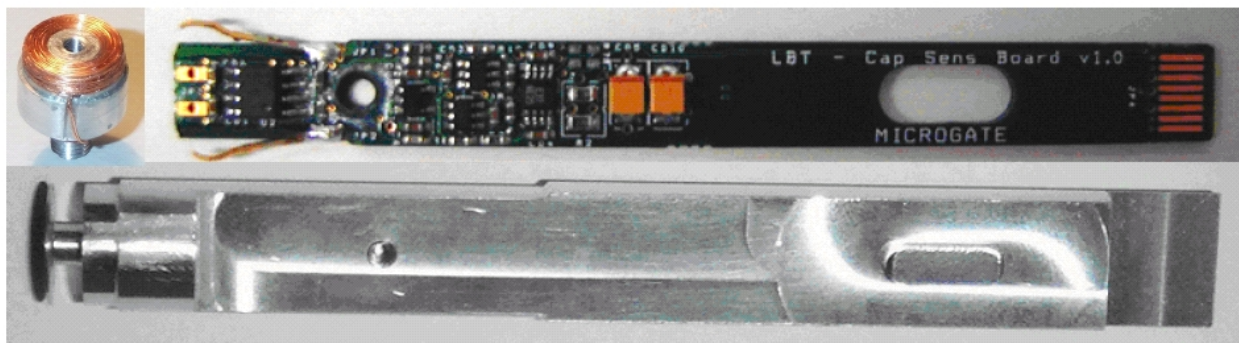


Figure 11-7. Components of the LBT actuator. Upper left: electromagnet coil head, 11 mm in diameter. Upper right: capacitive sensor board, 95 mm long, to be mounted on cold finger. Bottom: 108 mm cold finger.

The current driver for the electromagnet has a -3dB bandwidth of 300 kHz. It is commanded digitally at about 100 kHz with a resolution equivalent to 40 μ N. The maximum actuator force is 1.3 N. (Ref. 9)

The LBT secondary contains the digital signal processors (DSPs) that perform the wavefront reconstruction, calculate a feed-forward force command for each actuator, and control the actuators. The reconstructor and feed-forward calculations are distributed over the full set of DSPs. The computation time for these calculations is 34 μ s for the LBT secondary with 672 actuators and 707 subapertures. (Ref. 9)

The increase in diameter from 911 mm (LBT) to 1063 mm (GMT segment) has an impact on the actuator design. The spacing increases from 31 mm to 36 mm, allowing use of larger permanent magnets on the rear surface of the shell. This increases the efficiency of the electromagnet actuator by about 25%, allowing the shell to be made thicker (stiffer) for the same average actuator power. The precise shell thickness has not been determined but we take as a baseline 2.4 mm, 50% thicker than the LBT shell and 20% thicker than the MMT shell. At this thickness

gravitational print-through of the actuators is negligible at 1 nm rms. The thicker shell will also be less fragile than the LBT shells. While this effect is hard to quantify, it is clearly an advantage.

The actuator force and power requirements are reduced by incorporating bias magnets in each actuator, as is done for the LBT secondaries. A permanent magnet installed in each actuator body acts on the corresponding magnet attached to the shell to support ~85% of the local weight when at zenith. At 60° elevation angle the actuators no longer support any of the shell's weight, and below that they must on average push rather than pull. Because the actuator power dissipation goes as the square of the force, the permanent magnet greatly reduces the total power requirement.

We have calculated the average power required to correct for the atmosphere in 0.6" FWHM seeing and support 15% of the weight of the shell and its permanent magnets. The total heat dissipation of the ASM is about 17 kW. Each actuator dissipates 500 mW for a 4600-actuator total of 2.3 kW. The electronics in the chassis dissipate an additional 15 kW. Most of the actuator heat is extracted by the coolant circulating through the actuator mounting plate. Heat exchangers in the electronics chassis will remove the heat from those sources.

A modified lateral restraint needs to be developed for the GMT segments' shells, because the six outer segments have no central hole. This could be a set of three tangent rods bonded to the rear surface of the shell at an appropriate radius. Alternatively it could be a central ring of 40-60 mm diameter bonded to the rear surface. The lateral restraint membrane could attach to the ring in the same way it attaches to the inner edge of the LBT shells. At least one central actuator would be given up.

11.3.5 Control

The job of the ASM is to maintain the flatness of the optical wavefront over a bandwidth of approximately 1 kHz. The primary source of disturbance is atmospheric turbulence, with a significant additional source from wind-driven vibration of the telescope structure. The dynamic response analysis shows that the main concern from the wind is a group of structural modes in the range 8-10 Hz. Slow changes caused by gravity and temperature changes will also be corrected initially by the ASM before being off-loaded to the segment-positioning actuators.

The basic elements of the control system for the ASM are identical to those for the LBT adaptive secondaries. (Ref. 9) The electromagnet force actuators and capacitive displacement sensors combine to make a set of fast position actuators with a step-response settling time of about 0.5 ms and a precision of 2-3 nm. The absolute accuracy is limited by the wavefront sensor in adaptive mode and the shape of the reference body in seeing-limited mode. The control of the actuators uses a combination of open-loop feed-forward force commands and servo control with feedback from the capacitive sensors. The role of damping is critical in achieving the high bandwidth.

The reconstructor algorithm produces a set of displacement commands at a nominal 1 kHz rate determined by the wavefront sensor. The feed-forward force commands are the forces that would cause a static deflection equal to the desired displacements, obtained by multiplying the

displacements by a stiffness matrix. These force commands are sent directly to the current drivers open-loop. The servo portion of the actuator control loop runs at a rate of about 100 kHz, sampling the capacitive sensor and commanding the current driver. It uses a proportional-derivative algorithm, the derivative term serving to damp oscillations and allow the proportional gain to be set very high to give maximum response.

The feed-forward portion of the system depends on knowledge of the stiffness matrix that maps a vector of 672 displacements (at the actuator locations) to a vector of 672 forces. This is a stable matrix that can be calculated to high accuracy. Its inverse, the mapping from force command to displacement, will be measured in the lab as described in Section 11.3.8. This measurement automatically includes the actuator's force calibration, i. e. the relation between current and force.

The vibration modes of the shell have resonant frequencies ranging from about 30 Hz (astigmatism) to about 6 kHz (highest modes controlled by 672 actuators). The bandwidth of the DM's control system is full of resonances, and its performance depends strongly on damping with high bandwidth. The proportional servo gain (effectively the stiffness of the actuators, in N/ μm) that can be achieved without oscillation, and the control bandwidth, increase with the damping coefficient. The MMT adaptive secondary relies on mechanical damping from viscous flow of the air in the 50 μm gap between the shell and the reference body. The system has a step-response settling time of 1.7 ms. Air damping depends strongly on the gap size ($\propto 1/\text{gap}^3$). The necessarily small gap limits actuator stroke, eliminating the possibility of chopping. The LBT secondaries use electronic damping instead, implemented in the derivative term of the 100 kHz control loop. Its effectiveness is nearly independent of gap and its high bandwidth allows the settling time to be reduced to about 0.5 ms. The control system is being evaluated with a 45-actuator prototype of the LBT secondary, shown in Figure 11-8.

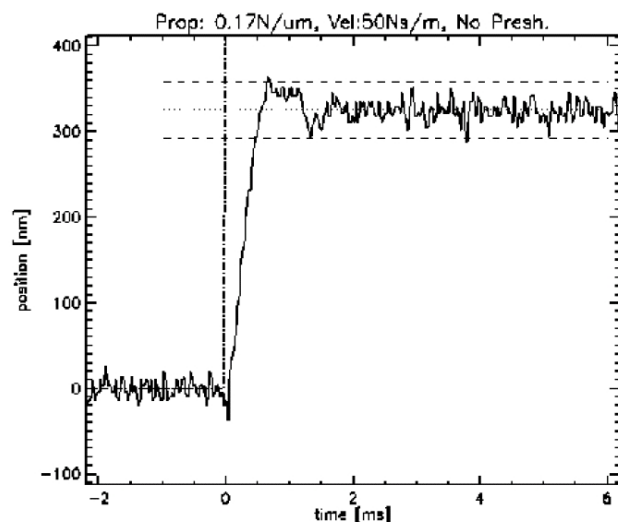
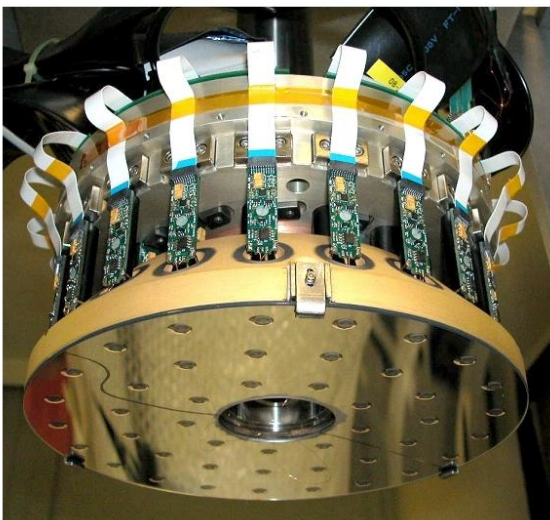


Figure 11-8. Left: 45-actuator prototype of LBT secondary. Right: measured response to a 325 nm step command for one actuator in a similar 36-actuator prototype. The settling time is 0.5 ms.

The most demanding requirement for the ASM is to reduce the effect of wind shake to 50 nm rms wavefront error, and 30 nm rms for extreme contrast AO. This is equivalent to residual

image motion of 1-1.7 mas. In the 75th percentile wind conditions the predicted motion is 40 mas before correction, dominated by frequencies in the 8-10 Hz range. This must be suppressed by a factor of 24-40. With a step response time of 0.5 ms, the ASM can achieve this suppression. Its internal control accuracy of 2-3 nm is a small fraction of the desired 30-50 nm rms. Achieving the desired suppression depends on the wavefront sensing as well as the ASM. The ASM will not limit the performance of the adaptive optics system.

11.3.6 Manufacture

The adaptive secondaries for the MMT and LBT have been manufactured by a collaboration between two Italian firms, Microgate and ADS, Steward Observatory, and Arcetri Observatory. Microgate has designed and assembled the electronics and DSP systems. ADS has designed and built the mechanical components, including the actuators apart from the capacitive sensor boards. Steward has made the Zerodur shells and reference bodies. Arcetri is integrating the full system for the LBT secondaries, and conducting laboratory tests and characterization. This arrangement has worked well with the major exception that two LBT shells were lost through accidents in manufacture and handling. (See Section 11.3.9.) Steward is making replacement shells and instituting strict procedures to reduce the risk of similar accidents in the future.

Manufacture of the mechanics and electronics is straightforward. Various options are available for manufacture of the shell and reference body. The process outlined below is based on that used for the LBT secondaries. It has been modified to produce the aspheric surfaces on the back of the shell and front of the reference body, and for efficient production of a large number of identical parts.

The segments and reference bodies will be made of zero-expansion material, probably Zerodur. The basic manufacturing plan for the shells is to produce the optical surface on a thick (roughly 75 mm thick) meniscus blank, then thin the blank from the rear surface to produce a shell of constant thickness. The shell may deform by many microns as it is thinned and loses its stiffness. This has no impact on the wavefront accuracy, which will be determined by the actuators, but it complicates the task of figuring the rear surface to match the reference body. The goal for the rear surface is to make it match the reference body within 25 μm peak-to-valley *when the optical surface is held in its accurate shape by the actuators*. This can be achieved by figuring the rear surface on the basis of thickness measurements rather than figure measurements. If the shell is made to have constant thickness within 10 μm , then when the optical surface is brought into the correct shape the rear surface will have the correct shape within 10 μm .

A possible sequence of operations for a GMT segment is as follows. Several of these steps would proceed in parallel.

1. The mirror blank for the shell is initially about 75 mm thick and 1160 mm in diameter. This diameter is maintained through the figuring operations on the front and rear surfaces in order to provide lap support at the edge.
2. The aspheric front surface is machined with a computer-controlled mill, and lapped with loose abrasives to an accuracy of about 5 μm rms. It is then polished to an accuracy of about

1 μm rms. The surface is measured with a laser tracker or a coordinate measuring machine (CMM).

3. The optical surface is figured to the specified accuracy. It is measured with an interferometer at its center of curvature, using a holographic null corrector to compensate for the asphericity. The test is described below.
4. The optical surface is attached with a thin layer of pitch to a matching convex blocking body of Zerodur.
5. Material is machined off of the rear surface to near the final thickness. The final stage of machining is performed with the computer-controlled mill to match the aspheric front surface. The shell is then lapped and polished to the final thickness and figure. The guiding measurement is shell thickness measured with an ultrasonic gauge.
6. The blocked shell is mounted on an edging mill and trimmed to the final diameter.
7. The shell is removed from the blocking body with a special fixture to support it. The blocked assembly is heated to melt the pitch and allow the shell to slide off of the blocking body.

Separately, the Zerodur reference body is made with a combination of machining and lapping processes. The 672 holes are made by core-drilling with a computer-controlled mill. The aspheric front surface and the spherical rear surface are machined, lapped and polished. The figure can be measured with a laser tracker or CMM to an accuracy of a few μm rms, adequate to match the rear surface of the shell within the specified 25 μm peak-valley.

It is essential that the manufacturer of the shells and reference bodies follow a careful, documented procedure for each step of the process. Critical processes, including all that involve the shell at its final thickness or close to that thickness, must be developed and demonstrated on prototype pieces.

Each secondary mirror segment has an aspheric departure of 1.7 mm peak-to-valley. It can be measured optically from its center of curvature using a single transmissive computer-generated hologram as a null corrector. This is in contrast to the primary segments whose 14 mm asphericity requires reflections off of two spherical mirrors in addition to the hologram. Figure 11-9 shows a preliminary design for the measurement. The hologram has an elliptical pupil, 136 mm x 100 mm, sized so that it can be manufactured with established techniques using either an advanced laser writer or electron-beam lithography. A nominal line spacing of 20 μm will provide adequate separation between the orders of diffraction. The hologram can be fabricated with 0.1 μm pattern distortion, which causes only 3 nm surface error in the measurement of the secondary segment. Figure 11-10 shows a hologram of the same size used to measure a 1.6 m off-axis parabolic mirror.

Because the null corrector consists of a single element, the segment's radius of curvature can be measured to an accuracy of better than 0.1 mm with a distance measurement using a laser tracker. Measurements of both figure and radius will be extremely repeatable through the sequence of off-axis segments because they rely on a common hologram.

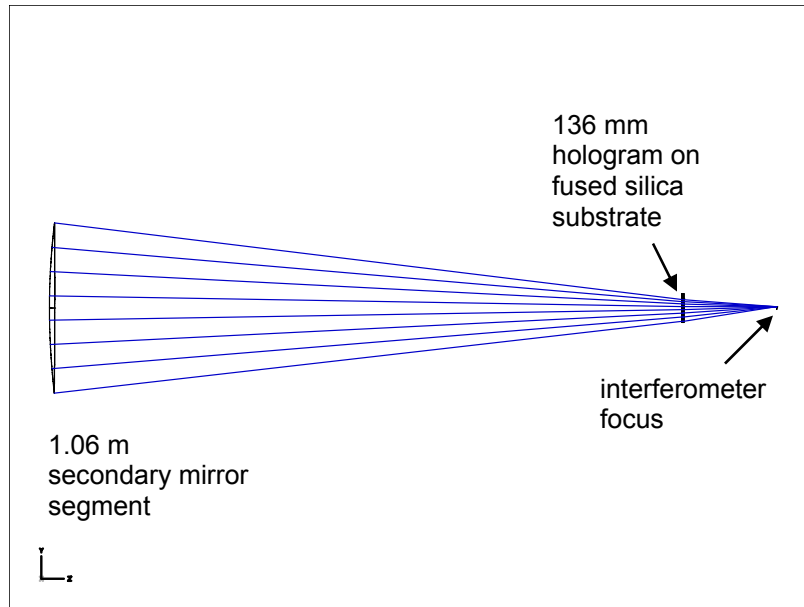


Figure 11-9. Preliminary design for a center-of-curvature measurement of the secondary mirror segment. A transmissive hologram serves as the null corrector.

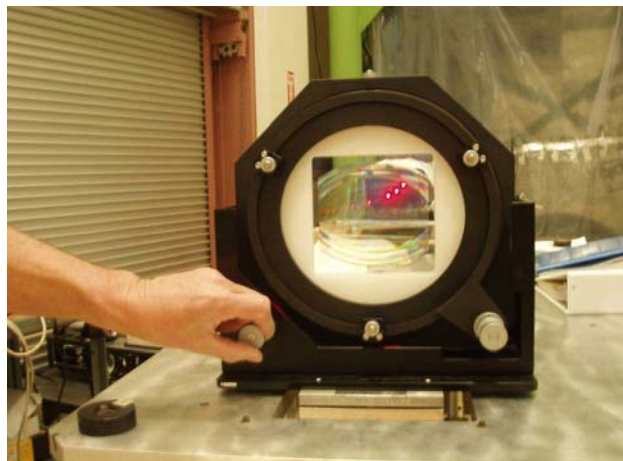


Figure 11-10. Computer-generated hologram used as a null corrector for a center-of-curvature test of a 1.6 m off-axis paraboloid at the University of Arizona Optical Sciences Center. The null corrector for the GMT segment is similar in size and design.

11.3.7 System integration

The ASM is a complex system that will require extensive characterization, tests, and fine-tuning of the hardware after it is manufactured. Similar development of the LBT adaptive secondaries is being carried out at Arcetri. (Ref. 7) Laboratory tests of the GMT's ASM will include electro-mechanical tests of the response to commands, both for individual actuators and for coordinated motion from tilt through high-order bending modes. They will also include optical tests and calibration, described in Section 11.3.8.

Interfaces between the ASM and the rest of the telescope must be defined in several areas. The mechanical interface is at the attachment of the triangular main frame to the OSS. Routine

installation and removal of the ASM will be done at that interface, i. e. the triangular main frame will remain with the ASM. The mass of the removable structure is approximately 4900 kg with CFRP frames.

The ASM is being designed so that no more than 20 kW is required for the full system, including actuators and electronics. The power consumption dictates the cooling requirement. The system is cooled by circulating coolant through the copper tubes in the actuator mounting plate. The 20 kW heat load requires 130 L/min of a 50% mixture of ethylene glycol and water at 2 K below ambient temperature. The entire coolant flow may be supplied by an external pump through lines running up the legs of the OSS, or the external system may supply a smaller flow at lower temperature, with a mixing valve and secondary loop on the ASM.

11.3.8 Calibration and testing

The Gregorian configuration allows optical measurements of the secondary mirror between two real conjugates. Direct interferometric wavefront measurements can be made as well as a measurement using an artificial star and the adaptive optics wavefront sensor. These are extremely valuable capabilities for the ASM in particular. The GMT will support these measurements in the telescope and in a thermally controlled laboratory at the telescope site. In the telescope version, a fiber point source with a diverging lens will be inserted at the prime focus, 2.3 m from the secondary mirror. It will illuminate a single segment at $f/2.1$ or the full secondary mirror at $f/0.7$. This serves as an artificial star for any sensor near the focal plane, including the adaptive optics wavefront sensor. This measurement will be made with the telescope at a fixed position, and the artificial star will be supported from a fixed structure in the enclosure. Fine alignment of the system will be done by moving the secondary mirror with the main actuators. The artificial star must be held stationary to about $9\ \mu\text{m}$, equivalent to 0.1" pointing stability, over short periods.

The laboratory tests will be similar to the tests of the LBT secondaries for which a test chamber has been prepared at Arcetri. (Ref. 7) In addition to the artificial star, the lab tests will include an interferometric wavefront measurement made with an interferometer at the far conjugate of the ellipsoidal secondary (approximately the Gregorian focus) and retroreflecting optics at the near conjugate. The retroreflecting optics may consist of a fast lens that images the secondary mirror onto a flat mirror, preserving the pupil imaging through two reflections off the secondary and onto the interferometer's detector. A beamsplitter or pick-off mirror can be inserted in front of the interferometer to deflect light to the adaptive optics wavefront sensor. Figure 11-11 shows the configuration for laboratory tests. The optical path is folded to fit the system into a volume of $3.5 \times 5 \times 14\ \text{m}^3$. This volume will have its temperature controlled to a few tenths of a K to allow accurate wavefront measurements.

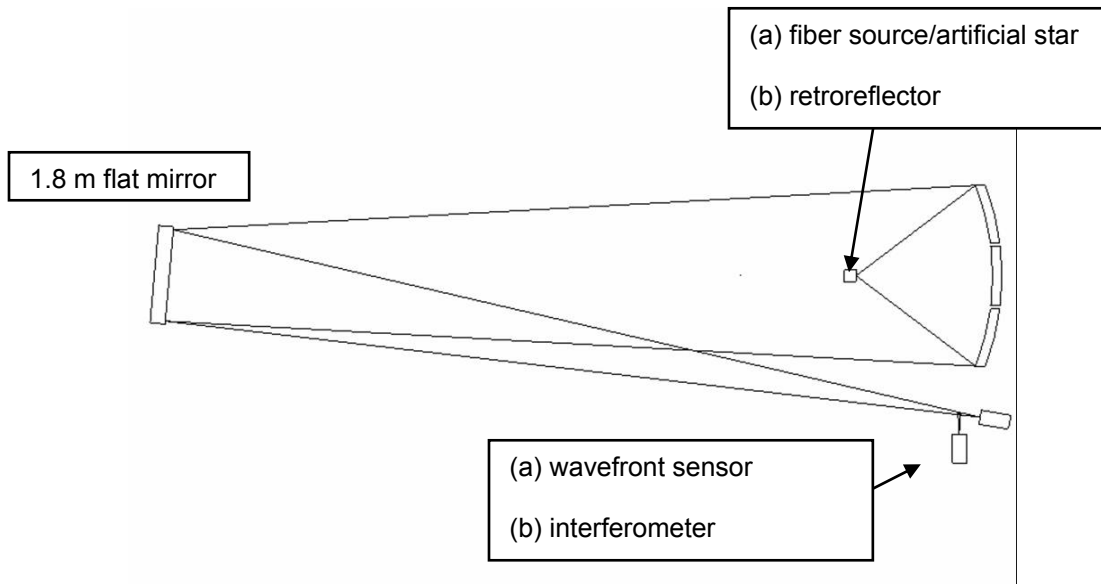


Figure 11-11. Layout of the optical test of the secondary mirror and wavefront sensors.

The test system will be used to calibrate and characterize both the ASM and the wavefront sensor. The calibration of the capacitive sensors will be verified by wavefront measurements over the full range of travel. Actuator influence functions (deflections over the full surface for unit commands to individual actuators) will be measured in order to verify or refine the calculated interaction matrix. The interaction matrix will be inverted to solve for the commands that flatten the wavefront—the fixed commands for seeing-limited operation—and these will be refined through iteration. The response of the wavefront sensor to controlled wavefront slopes will also be measured. The entire adaptive optics system will be evaluated extensively, including closed-loop operation that tests the hardware and software.

11.3.9 Technical challenges and risks

The primary risks in building the ASM are: fabrication and handling of the shells; actuator reliability; integration and testing; and the fact that there is currently only one commercial source for the electronics. The first three are both programmatic and technical risks while the fourth is purely programmatic. The technical risks are mitigated by the experience gained through the MMT and especially the LBT secondaries.

Accidents that led to the loss of two LBT shells establish that this is an area of high risk to the GMT's ASM with its seven shells. The experience, however, has led to stringent procedures that reduce the risk of similar accidents. The figuring and thinning of both shells was completed successfully. The first shell was lost while it was being trimmed to the final diameter. Following a set of experiments, the trimming procedure was modified to prevent high loads. The cut is now made with a downward tool motion through the shell rather than a radial feed. This process was successful on the second shell. This shell, however, was damaged during packing or shipment to Italy in November 2005. The design and procedure for packing shells is being evaluated, and modifications will be made before the replacement shells are shipped.

Before shells are manufactured for the ASM, all critical aspects of the process will be demonstrated on prototype shells. At the same time, the project plans for the possibility that some shells, and possibly some reference bodies, will be lost through accidents during manufacture, integration with the actuator system, and use at the telescope. The initial procurement will be for at least eight shells and seven reference bodies for the outer segments and two of each for the center segment. Provisions will be made to maintain the processes and equipment to make more shells and reference bodies if necessary.

Actuator reliability needs to be demonstrated for the specific GMT design that will be developed in future phases of the project. The performance of the MMT actuators (seven failures during commissioning, followed by zero failures in two years of operation) would meet the GMT goal of 100,000 hours between failures.

Development of procedures for integration and testing will benefit greatly from the experience with the LBT secondaries. The control algorithm and much of the software will be common to the LBT system. A small prototype similar to the LBT 45-actuator prototype will be built and used to characterize all electro-mechanical aspects of the system. Integration and testing will follow the same procedures being developed for LBT, using the optical test facility described in Section 11.3.8 that has the same capabilities.

There is concern that the electronics for adaptive secondary mirrors are currently being produced by only one company (Microgate). Microgate has been involved in developing and producing adaptive secondary mirrors and related systems for more than 10 years, and has provided continuous and reliable service to a number of astronomy organizations, including Steward Observatory, LBT, ESO, Keck and Gemini. While the adaptive secondaries are an important part of Microgate's business, the company does not rely on them alone. We are confident that Microgate will be available to propose work for the ASM, but we will continue to address this issue during the design and development of the ASM.

11.4 Fast-steering secondary mirror

11.4.1 Overview

The FSM is segmented like the ASM, but made of rigid lightweighted Zerodur segments. The FSM segments have about one-third the mass of the ASM segments. If the rest of the FSM assembly—including frames and actuators—is identical to the ASM assembly, it will weigh about 1700 kg less than the ASM assembly. It will have the same mechanical interfaces as the ASM to allow for quick installation and removal. Common parts and electronics will be used as much as practical for both systems as well.

Rapid correction of wind-induced vibration and tracking jitter will be made with the fine-positioning actuators described in Section 11.2. We expect that feedback from the tilt sensor in the focal plane, without additional signals from accelerometers, will be adequate to reduce the vibration by the modest factor required for seeing-limited observations.

11.4.2 Requirements

The requirements for the FSM, listed in Table 11-5, are taken from the image and wavefront budgets in Chapter 12. The relevant requirements are the secondary segment figure and secondary segment support errors. Requirements related to active alignment and suppression of wind disturbances are applied to the secondary mirror mount (Section 11.2). The segment figure errors include polishing and testing errors. Like the primary figure errors (Chapter 10), these are specified as a structure function corresponding to the given image size. The support errors, specified simply as the contribution to the image size, include gravity sag over zenith angles between 0 and 60°, and support force errors.

Table 11-5. Specifications and goals for manufacture and support of the FSM segments, in terms of image diameter containing 80% of the light at 500 nm.

type of error	θ_{80} (arcsec)	
	specification	goal
segment figure	0.039	0.026
segment support	0.020	0.020
sum in quadrature	0.044	0.033

11.4.3 Segment design

The structure of the Zerodur segments is shown in Figure 11-12 for the current design. The dimensions are listed in Table 11-6.

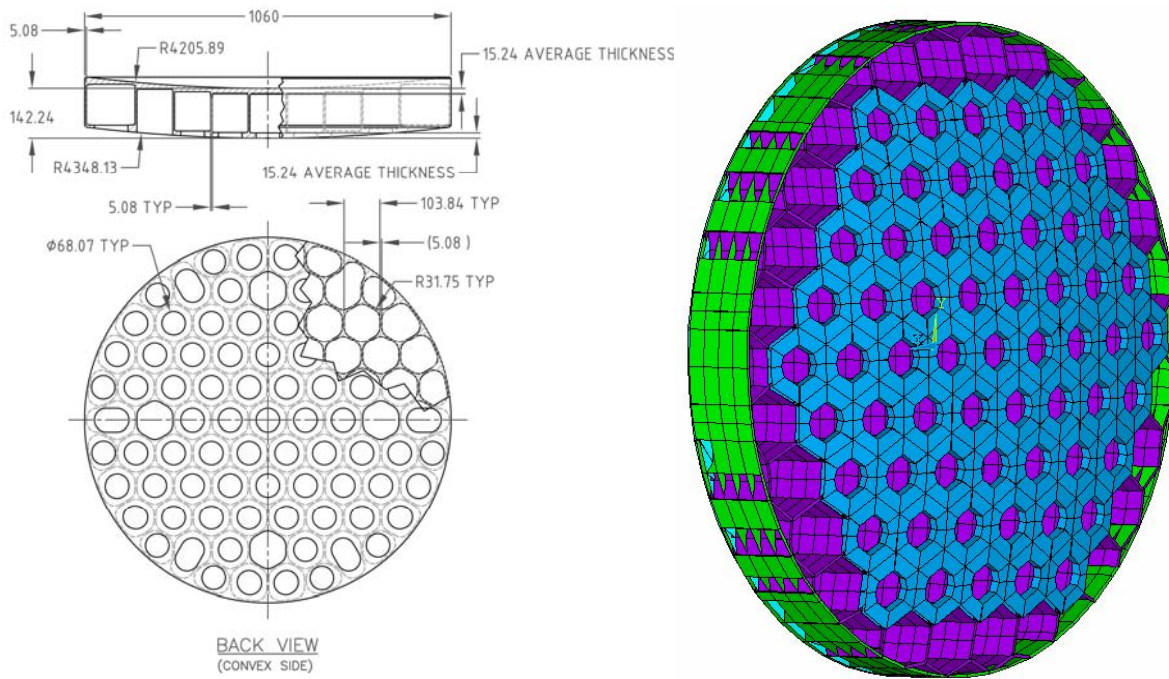


Figure 11-12. Structure of the Zerodur FSM segments. Dimensions are in mm.

Table 11-6. Dimensions of the FSM segments.

shape	meniscus
mass	107 kg
center of gravity	22 mm behind vertex
moment of inertia	9.31 kg-m ²
face and back thickness	15.2 mm
web and outer cylinder thickness	5.1 mm
hex cell spacing	104 mm
overall thickness	142.2 mm

The segment is supported by the 6 fine-positioning actuators. In the current design they are attached to the rear surface of the segment at 6 points with no load spreaders. We have analyzed this structure and shown that it meets the requirement for support errors comfortably at zenith but only marginally at 60° from zenith. Further work will be performed during the preliminary design phase to reduce the deflections at 60°.

A preliminary analysis indicates that the forces applied to compensate for telescope vibration can be reacted by the telescope structure, without causing significant parasitic motion of the structure. We will evaluate the performance further during the preliminary design phase and, if necessary, introduce a compensating mechanism with counterweights.

11.4.4 Segment manufacture

The lightweighted segment blanks will be obtained from Schott and are similar to other lightweighted Zerodur mirrors cast and machined by Schott, including the 1.3 m f/11 secondaries for the Magellan telescopes. We expect that the figuring requirement can be met by a number of modern processes; relatively large slope errors are allowed because of the factor-of-8 scaling from the secondary mirror to the telescope pupil. The goal of $\theta_{80} = 0.026''$ matches the accuracy of the Magellan f/11 secondaries. Each segment can be measured from its center of curvature using a computer-generated hologram for a null corrector, as described for the ASM in Section 11.3.6.

The hologram provides both an optical and a mechanical reference for measurement of the segment's radius of curvature with a laser tracker. Using the tracker in its interferometric mode, we expect to be able to control the radii of the seven segments within 50 μm , the requirement for matching. The hologram can also project alignment references onto the segment that will allow control of its off-axis distance and clocking within 200 μm or better.

11.5 References

1. P. Salinari, C. Del Vecchio and V. Biliotti, 1993. "A study of an adaptive secondary mirror", in *Active and Adaptive Optics*, ed. F. Merkle, Proc. ICO-16 Satellite Conference 48, p. 247 (Garching: International Commission for Optics).
2. P. Salinari and D. G. Sandler, 1998. "High order adaptive secondary mirrors: Where are we?", in *Adaptive Optical System Technologies*, ed. D. Bonaccini and R. K. Tyson, SPIE 3353, p. 742.
3. G. Brusa, A. Riccardi, S. Ragland, S. Esposito, C. Del Vecchio, L. Fini, P. Stefanini, V. Biliotti, P. Ranfagni, P. Salinari, D. Gallieni, R. Biasi, P. Mantegazza, G. Sciocco, G. Noviello and S. Invernizzi, 1998. "Adaptive secondary P30 prototype: laboratory results", in *Adaptive Optical System Technologies*, ed. D. Bonaccini and R. K. Tyson, SPIE 3353, p. 764.
4. M. Lloyd-Hart, 2000. "Thermal Performance Enhancement of Adaptive Optics by Use of a Deformable Secondary Mirror", *PASP* 112, p. 264.
5. A. Riccardi, G. Brusa, V. Biliotti, C. Del Vecchio, P. Salinari, P. Stefanini, P. Mantegazza, R. Biasi, M. Andrighttoni, C. Franchini, D. Gallieni, M. Lloyd-Hart, P. C. McGuire, S. M. Miller and H. M. Martin, 2000. "The adaptive secondary mirror for the 6.5m conversion of the Multiple Mirror Telescope: latest laboratory test results of the P36 prototype", in *Adaptive Optical System Technologies*, ed. P. L. Wizinowich, SPIE 4007, p. 524.
6. G. Brusa, A. Riccardi, P. Salinari, F. Wildi, M. Lloyd-Hart, H. M. Martin, P. Mantegazza, R. Biasi, D. Gallieni and F. Zocchi, 2003. "MMT adaptive secondary: performance evaluation and field testing", in *Adaptive Optical System Technologies II*, ed. P. L. Wizinowich and D. Bonaccini, Proc. SPIE 4839, p. 691.
7. A. Riccardi, G. Brusa, P. Salinari, D. Gallieni, R. Biasi, M. Andrighttoni and H. M. Martin, 2003. "Adaptive secondary mirrors for the Large Binocular Telescope". in *Adaptive Optical System Technologies II*, ed. P. L. Wizinowich and D. Bonaccini, SPIE 4839, p. 721.
8. R. Biasi, M. Andrighttoni, D. Veronese, V. Biliotti, L. Fini, A. Riccardi, P. Mantegazza and D. Gallieni, 2003. "LBT adaptive secondary electronics", in *Adaptive Optical System Technologies II*, ed. P. L. Wizinowich and D. Bonaccini, SPIE 4839, p. 772.
9. R. Biasi, M. Andrighttoni, A. Riccardi, V. Biliotti, L. Fini, P. Mantegazza and D. Gallieni, 2004. "Dedicated flexible electronics for adaptive secondary control", in *Advancements in Adaptive Optics*, ed. D. Bonaccini Calia, B. L. Ellerbroek and R. Ragazzoni, SPIE 5490, p. 1502.
10. L. M. Close, F. Wildi, M. Lloyd-Hart, G. Brusa, D. Fisher, D. Miller, A. Riccardi, P. Salinari, D. W. McCarthy, R. Angel, R. Allen, H. M. Martin, R. G. Sosa, M. Montoya, M. Rademacher, M. Rascon, D. Curley, N. Siegler and W. J. Duschl, 2003. "High Resolution Images of Orbital Motion in the Trapezium Cluster: First Scientific Results from the MMT Deformable Secondary Mirror Adaptive Optics System", *Ap. J.* 599, p. 537.

11. P. M. Hinz, J. R. P. Angel, N. J. Woolf, W. F. Hoffmann and D. W. McCarthy, 2000. SPIE 4006, p. 349.
12. W. F. Hoffmann, J. L. Hora, G. G. Fazio, L. K. Deutsch and A. Dayal, 1998. SPIE 3354, p. 647.
13. M. Freed, P. M. Hinz, M. R. Meyer, N. M. Milton and M. Lloyd-Hart, 2004. SPIE 5492, p. 1561.
14. D. W. McCarthy, J. Burge, R. Angel, J. Ge, R. Sarlot, B. Fitz-Patrick and J. Hinz, 1998. SPIE 3354, p. 750.